JBC RESEARCH ARTICLE

Phagocytosis mediated by the human granulocyte receptor CEACAM3 is limited by the receptor-type protein tyrosine phosphatase PTPRJ

Received for publication, April 22, 2022, and in revised form, July 4, 2022 Published, Papers in Press, July 16, 2022,
https://doi.org/10.1016/j.jbc.2022.102269

Griseldis Goob[1], **Jonas Adrian**[1], **Chiara Cossu**[1], **and Christof R. Hauck**[1,2,*]

From the [1]*Lehrstuhl Zellbiologie, Fachbereich Biologie, and* [2]*Konstanz Research School Chemical Biology, Universität Konstanz, Germany*

Edited by Phyllis Hanson

Carcinoembryonic antigen-related cell adhesion molecule 3 (CEACAM3) is a human granulocyte receptor mediating the efficient phagocytosis of a subset of human-restricted bacterial pathogens. Its function depends on phosphorylation of a tyrosine-based sequence motif, but the enzyme(s) responsible for reversing this modification are unclear. Here, we identify the receptor-type protein tyrosine phosphatase PTPRJ as a negative regulator of CEACAM3-mediated phagocytosis. We show depletion of PTPRJ results in a gain-of-function phenotype, while overexpression of a constitutively active PTPRJ phosphatase strongly reduces bacterial uptake *via* CEACAM3. We also determined that recombinant PTPRJ directly dephosphorylates the cytoplasmic tyrosine residues of purified full-length CEACAM3 and recognizes synthetic CEACAM3-derived phosphopeptides as substrates. Dephosphorylation of CEACAM3 by PTPRJ is also observed in intact cells, thereby limiting receptor-initiated cytoskeletal re-arrangements, lamellipodia formation, and bacterial uptake. Finally, we show that human phagocytes deficient for PTPRJ exhibit exaggerated lamellipodia formation and enhanced opsonin-independent phagocytosis of CEACAM3-binding bacteria. Taken together, our results highlight PTPRJ as a bona fide negative regulator of CEACAM3-initiated phagocyte functions, revealing a potential molecular target to limit CEACAM3-driven inflammatory responses.

Phagocytosis is an important cellular defense mediated by professional phagocytes including granulocytes, macrophages, and dendritic cells. Dedicated phagocytic receptors, such as Fc-receptors, complement receptors, scavenger receptors, carcinoembryonic antigen-related cell adhesion molecule 3 (CEACAM3), or dectin-1, play a central role in this process (1). While Fc-receptors and complement receptors require prior opsonization, CEACAM3 and dectin-1 directly bind to specific surface-exposed features of their target particles (2, 3). In contrast to dectin-1, which recognizes glycan moieties exposed on the yeast cell wall, CEACAM3 detects a specific functionality of various human-restricted bacterial pathogens: the possession of CEACAM-binding adhesins (4). The *CEACAM3* gene is only present in higher primates where expression of the protein is restricted to granulocytes (5). As a receptor with a narrow target spectrum, CEACAM3 appears to be involved in a molecular arms race with specialized human-restricted bacterial pathogens such as *Neisseria gonorrhoeae* (5, 6). Indeed, the extracellular IgV-like domain of CEACAM3 recognizes CEACAM-binding surface proteins of diverse microbes with the Opa proteins of *N. gonorrhoeae* serving as the best characterized CEACAM-binding adhesins (7–11). On the other hand, the functionality of CEACAM3 as a phagocytic receptor depends on a short sequence in its cytoplasmic domain reminiscent of an immunoreceptor tyrosine-based activation motif (ITAM). Similar to classic ITAM motifs found in Fcγ receptors or the T-cell receptor-associated zeta chain, phosphorylation of the two ITAM-embedded tyrosine residues (Y230 and Y241) of CEACAM3, which are the only tyrosine residues contained within the complete cytoplasmic domain of CEACAM3, depends on Src family protein tyrosine kinases (PTKs) (7, 12). This initial tyrosine phosphorylation allows association with the SH2-domain of the Rac guanine nucleotide exchange factor Vav accompanied by a rapid increase in GTP-loaded Rac and WAVE-complex-dependent cytoskeletal rearrangements (13–15). The resulting actin polymerization drives the local formation of prominent lamellipodia, a characteristic hallmark of CEACAM3-mediated phagocytosis (14, 16, 17). CEACAM3 tyrosine phosphorylation and Rac activity are also linked to the subsequent production of reactive oxygen species (18, 19). Accordingly, CEACAM3 tyrosine phosphorylation has to be tightly controlled, but the enzymes responsible for CEACAM3 dephosphorylation are currently unknown.

In the case of the TCR-ζ chain, the receptor-type protein tyrosine phosphatase (PTPR) PTPRJ, is able to dephosphorylate the ITAM tyrosine residues, thereby suppressing TCR signal transduction (20–22). On the other hand, the same enzyme also appears to act on the phosphorylated, carboxy-terminal tyrosine residue responsible for the autoinhibited state of Src family PTKs, thereby promoting Src PTK activity (23–25). This dual role of PTPRJ in enhancing Src family PTK

* For correspondence: Christof R. Hauck, christof.hauck@uni-konstanz.de.
Present address for Jonas Adrian: Cilag AG - JSC Schaffhusen, Hochstrasse 201, 8200 Schaffhausen, Switzerland.

activity and reducing phosphorylation of membrane proteins has also been observed in the case of other ITAM-containing receptors such as dectin-1 (26). Given this disparate function of PTPRJ on receptor-mediated signal transduction, it is not surprising that the *in vivo* ablation of this enzyme has yielded conflicting results. While genetic ablation of the PTPRJ phosphatase domain in the mouse results in early embryonic lethality, the recent report of biallelic loss-of-function variants indicates that the complete deletion of PTPRJ in humans is compatible with normal development (27, 28). However, PTPRJ deficiency in humans seems to impair platelet activity supporting a positive role of PTPRJ in platelet activation and thrombosis (29, 30).

Using a focused genetic screen, we here identify PTPRJ as a negative regulator of CEACAM3-mediated phagocytosis by human cells. While Src family PTK signaling is not affected, overexpression of PTPRJ diminishes tyrosine phosphorylation of the receptor and reduces CEACAM3-mediated internalization of bacteria. PTPRJ acts on both phosphorylated tyrosine residues within the CEACAM3 ITAM-like motif. CRISPR/Cas9-mediated deletion of PTPRJ in myeloid cells results in a "gain-of-function" phenotype consistent with an inhibitory role of PTPRJ on the human innate immune defense against human-restricted CEACAM3-binding microbes.

Results

A genetic screen of human PTPRs identifies tyrosine phosphatases with a negative role in CEACAM3-mediated phagocytosis

As a prerequisite for our genetic screen, we first generated a phagocyte cell line stably expressing CEACAM3 and a separate protein serving as selection marker. To this end, a CEACAM3-mKate fusion protein and the blue-fluorescent protein Cerulean were stably expressed in human myeloid HL60 cells (HL60-CEACAM3 cells; Fig. 1, *A*–*C*). Next, we individually disrupted each of the 20 human PTPR genes in HL60-CEACAM3 cells using lentiviral transduction of target-specific single guide RNAs (sgRNAs) together with Cas9 (see Fig. 1*D* for a schematic outline of the screening procedure). To limit the analysis to Cas9-modified cells, the HL60-CEACAM3 cells were cotransduced with a second lentiviral particle encoding a sgRNA targeting the Cerulean cDNA (Fig. 1*D*). As the sgCerulean-containing viral particles lack a Cas9 gene, disruption of the Cerulean reading frame can only occur, if a cell is coinfected by the sgPTPRx/Cas9-encoding virus and functionally expresses Cas9. One week after gene targeting, the different PTPR-deficient HL-60 cell lines were infected for 15 min with fluorescein-labeled *N. gonorrhoeae*. Uptake of the bacteria was quantified *via* flow cytometry by gating on the Cerulean-negative cells and measuring the fluorescein signal derived from internalized bacteria (Fig. 1*D*) (5, 31). Transduction of HL60-CEACAM3 cells with the Cerulean-targeting sgRNA did not compromise the efficient opsonin-independent internalization of Opa_{52}-expressing *N. gonorrhoeae*, which are recognized by CEACAM3 (Fig. 1*E*). Fluorescein-labeled, non-opaque *N. gonorrhoeae*, which are unable to bind CEACAM3, were not internalized by HL60-CEACAM3 cells, demonstrating that the observed rapid phagocytosis was CEACAM3 mediated (Fig. 1*E*). For most targeted PTPRs, no major changes in phagocytosis or a reduced uptake were observed as exemplified for PTPRD, PTPRN2, PTPRO, and PTPRR (Fig. 1, *F* and *H*). As the successful sgRNA-mediated gene disruption and resulting protein depletion was not determined for each PTPR at this point, we cannot rule out that samples lacking an effect on CEACAM3-mediated phagocytosis might represent false negatives. However, disruption of specific PTPR genes resulted in a gain-of-function with enhanced uptake of Opa_{52}-expressing *N. gonorrhoeae* by Cerulean-negative cell populations, and we focused our further study on these positive candidates (Fig. 1, *G* and *H*). Such a gain-of-function in CEACAM3-mediated phagocytosis was seen in cells with targeted disruption of PTPRJ, PTPRS, PTPRF, and PTPRG, four protein phosphatases known to be present in HL60 cells (32). This result implied that one or more of these four PTPRs could function as a negative regulator of CEACAM3-initiated events.

Overexpression of active PTPRJ diminishes CEACAM3-mediated phagocytosis

To directly test a potential negative role of PTPRF, PTPRG, PTPRJ, and PTPRS, we overexpressed these enzymes together with CEACAM3 using 293T cells, which lack endogenous expression of any CEACAM. In this case, we used the catalytic domains of the distinct phosphatases fused to a myristoylation signal directing the enzyme to the inner leaflet of the plasma membrane (Fig. 2*A*). With the exception of PTPRG, all phosphatase domains were expressed at equivalent levels and also a uniform expression of CEACAM3 was confirmed by Western blotting (Fig. 2*B*). As observed before, CEACAM3-expression allowed efficient uptake of Opa_{52}-expressing *N. gonorrhoeae* by 293T cells, while nonopaque gonococci were not internalized (Fig. 2*C*). Strikingly, only expression of myr-PTPRJ resulted in a strong reduction in CEACAM3-mediated bacterial internalization, while expression of myr-PTPRS, myr-PTPRF, or myr-PTPRG did not interfere with CEACAM3-mediated uptake (Fig. 1*C*). Myristoylated PTPRJ was indeed found associated with the plasma membrane, where it co-localized with CEACAM3 and CEACAM3-bound gonococci (Fig. 2*D*). In summary, these results suggested that in particular the receptor protein tyrosine phosphatase PTPRJ could constitute a negative regulator of CEACAM3-mediated phagocytosis.

PTPRJ diminishes CEACAM3 tyrosine phosphorylation

Upon bacterial engagement, the CEACAM3 cytoplasmic domain is rapidly tyrosine phosphorylated at the HemITAM sequence by active Src family kinases (12, 33). To examine if PTPRJ affects bacterial uptake by diminishing CEACAM3 phosphorylation or by interfering with Src kinase activity, we co-transfected 293T cells with constructs encoding CEACAM3-GFP or GFP together with either myr-PTPRJ wildtype or the catalytically inactive mutant myr-PTPRJ-D/A. Western

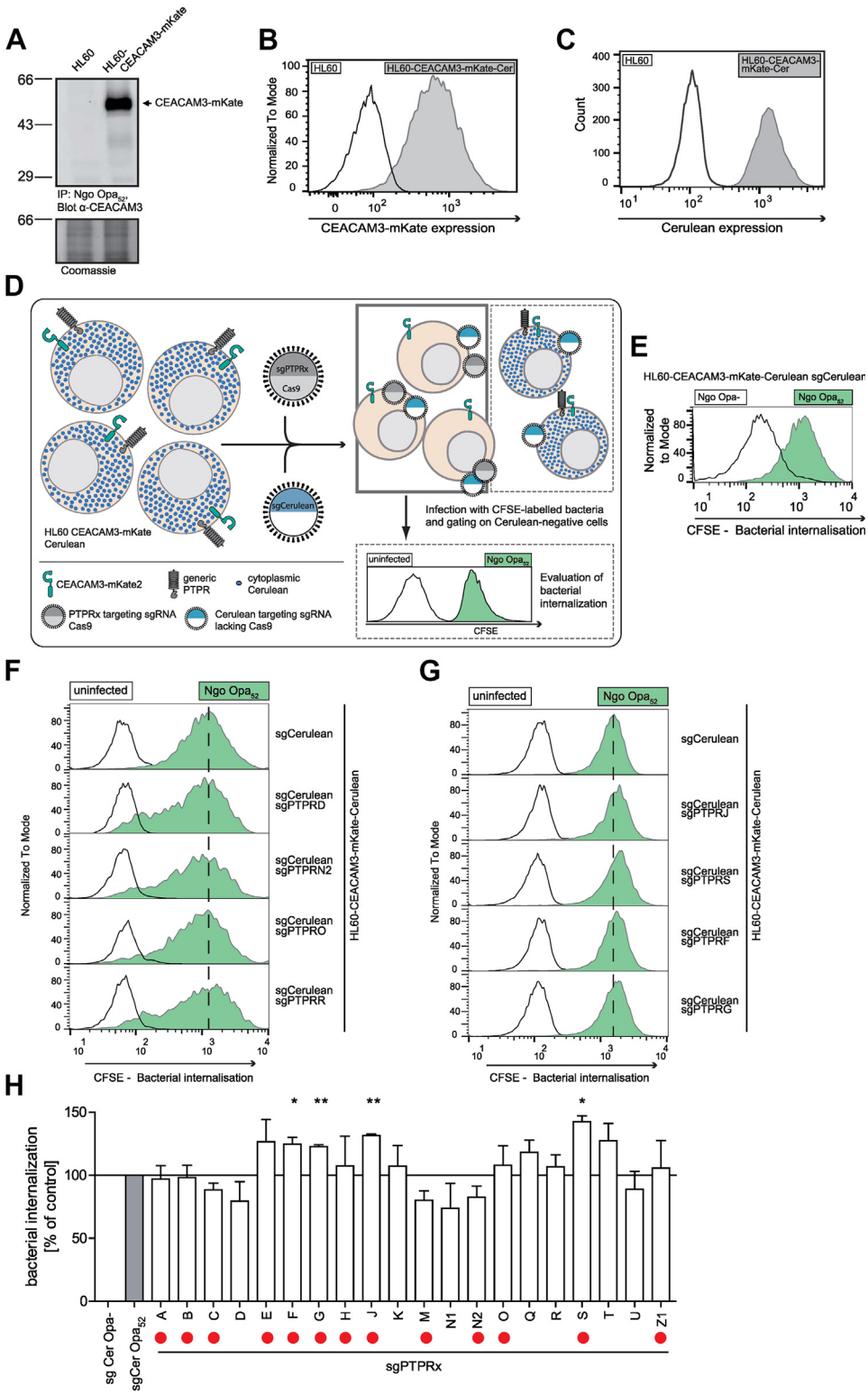

Figure 1. A genetic screen of human PTPRs identifies tyrosine phosphatases with a negative role in CEACAM3-mediated phagocytosis. *A,* lysates of HL60 wildtype or HL-60-CEACAM3-mKate2 cells were incubated with PFA-fixed Opa_{52}-expressing *N. gonorrhoeae,* and bound CEACAMs were precipitated. Precipitates were probed by Western blotting with α-CEACAM3 antibodies (*upper panel*). Coomassie staining demonstrates even protein loading of the lanes (*lower panel*). *B,* expression of CEACAM3-mKate in HL60-CECAM3-mKate Cerulean cells was confirmed by flow cytometry by measuring the mKate fluorescence. *C,* expression of Cerulean by HL60-CECAM3-mKate Cerulean cells was verified by flow cytometry. *D,* schematic representation of the focused CRISPR screen. HL60 CEACAM3-mKate Cerulean cells were transduced with a combination of two recombinant lentivirus particles. One contains a guide RNA sequence targeting one of the 20 receptor-like protein tyrosine phosphatases (sgPTPRx, *dark gray*) together with the Cas9-expression cassette (Cas9, *light gray*). The second viral particle contained a guide RNA sequence targeting the cerulean cDNA (sgCerulean, *blue*) without the Cas9-expression cassette. Consequently, a functional sgCerulean–Cas9 complex can only form in cells treated with both types of viral particles. By gating on the cerulean-negative population, the phagocytic potential of cells with compromised expression of one specific PTPR can be analyzed upon infection with CEACAM3-binding bacteria. *E,* HL60-CEACAM3-mKate cells, in which only cerulean was knocked out (HL60 CEACAM3-mKate control), were infected for 15 min with

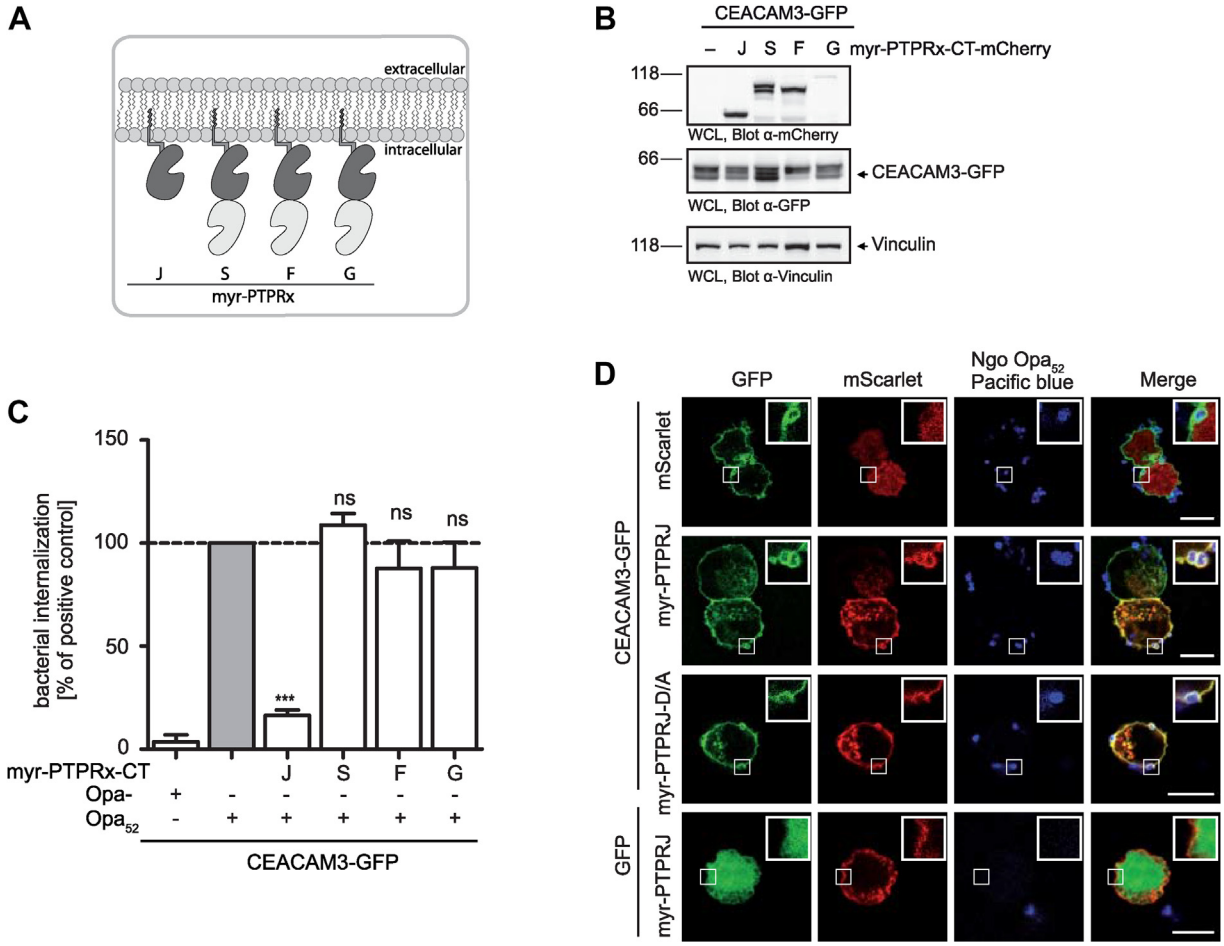

Figure 2. Overexpression of active PTPRJ diminishes CEACAM3-mediated phagocytosis. *A,* schematic representation of myristoylated (myr-) protein phosphatase domains lacking the extracellular and the transmembrane domain. PTPRS, PTPRF, and PTPRG harbor, in addition to the catalytically active phosphatase domain (*dark gray*), a second catalytically inactive domain (*light gray*). *B,* 293T cells were cotransfected to express CEACAM3-GFP together with the indicated phosphatase domains fused to mCherry. Equal CEACAM3-GFP expression levels and expression of the different myr-phosphatase-mCherry constructs were analyzed by Western blotting using α-GFP (*upper panel*) and α-mCherry (*middle panel*) antibodies. Probing of the samples with α-vinculin (*lower panel*) served as loading control. *C,* cells from (B) were infected with Opa_{52}-expressing (Opa_{52}) or Opa-negative (Opa-) *N. gonorrhoeae* (MOI 30) for 45 min. Internalized bacteria were enumerated by gentamicin protection assays. Bars show mean ± SEM of three independent experiments performed in triplicates. n.s., not significant; ***$p < 0.001$. *D,* 293T cells were cotransfected with plasmids encoding GFP-tagged CEACAM3 or GFP alone together with the indicated mScarlet-tagged myristoylated phosphatase domain or mScarlet alone. Cells were infected with PacificBlue-labeled Opa_{52}-expressing *N. gonorrhoeae* for 30 min, fixed, and analyzed by confocal microscopy. Insets show 3× magnification of boxed areas. Bars represent 10 μm (corresponding to 3.3 μm for insets). CEACAM3, carcinoembryonic antigen-related cell adhesion molecule 3; PTPR, receptor-type protein tyrosine phosphatase.

blot analysis confirmed the equivalent expression of CEACAM3-GFP and GFP (Fig. 3*A*). Likewise, myr-PTPRJ and myr-PTPRJ-D/A were expressed at similar levels (Fig. 3*A*). A low basal tyrosine phosphorylation of immunoprecipitated CEACAM3 could be observed, both in the absence of CEACAM3-binding bacteria and after infection with Opa-negative *N. gonorrhoeae* (Fig. 3*B*). As expected, infection with CEACAM-binding *N. gonorrhoeae* Opa_{52} resulted in a marked increase in CEACAM3 tyrosine phosphorylation (Fig. 3*B*). However, receptor phosphorylation was completely abolished, when the truncated, active myr-PTPRJ was co-expressed together with CEACAM3, whereas co-expression of the catalytically inactive myr-PTPRJ-D/A variant showed the opposite effect (Fig. 3*B*). Interestingly, expression of myr-PTPRJ did not alter the tyrosine phosphorylation state of c-Src, neither at the activation loop tyrosine residue Y-419 nor at the negative regulatory tyrosine residue Y-530 near the carboxy terminus of c-Src (Fig. 3*C*). The Y-530 residue of c-Src is dephosphorylated upon serum stimulation of cells, which is known to correspond to increased c-Src activity

CSFE-labeled nonopaque (Opa-) or Opa_{52}-expressing *N. gonorrhoeae* (Opa_{52}). Signals of extracellular bacteria were quenched by trypan blue, and the CSFE fluorescence derived from intracellular bacteria is depicted in the histograms. *F, G,* HL60-CEACAM3-mKate cells transduced with the indicated sgRNAs targeting individual PTPRs were left uninfected or were infected with CFSE-stained Opa_{52}-expressing *N. gonorrhoeae,* and bacterial internalization was measured as in (*E*). *H,* quantification of uptake experiments performed as in (*E*). Data are from three independent experiments and are normalized to the CFSE fluorescence detected upon infection of HL60 CEACAM3-mKate control cells with Opa_{52}-expressing *N. gonorrhoeae*. *Red circles* indicate PTPRs known to be expressed by HL60 cells. Bars represent mean ± SEM from three independent experiments. Statistically significant increases in bacterial internalization were determined by Student's *t* test and indicated by *asterisks*. *$p < 0.05$; **$p < 0.01$. CEACAM3, carcinoembryonic antigen-related cell adhesion molecule 3; CFSE, carboxyfluorescein succinimidyl ester; PTPR, receptor-type protein tyrosine phosphatase; sgRNA, single guide RNA.

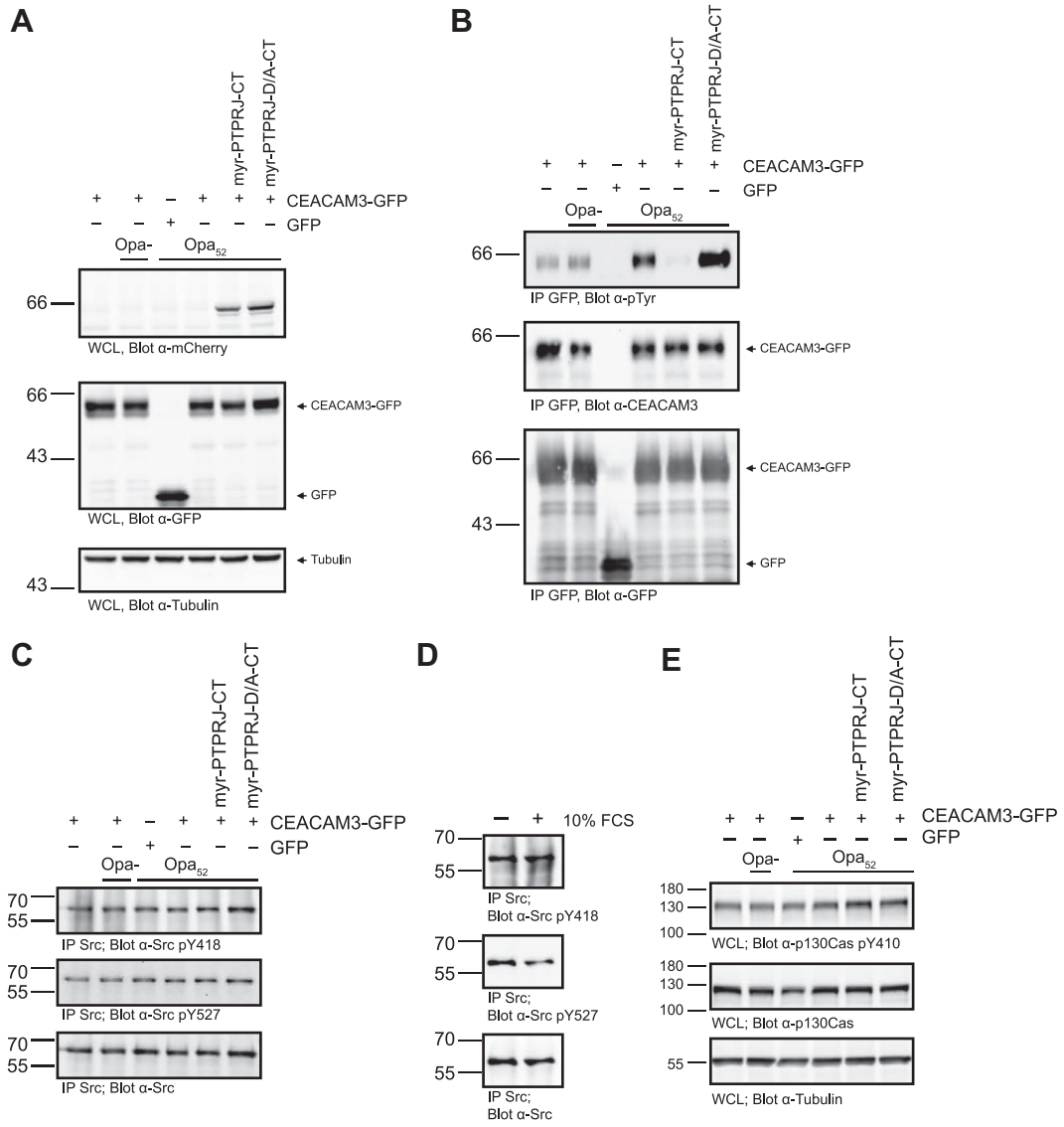

Figure 3. PTPRJ diminishes CEACAM3 tyrosine phosphorylation. *A,* 293T cells were transfected to express CEACAM3-GFP or GFP. Where indicated, cells were additionally transfected with constructs encoding the mCherry-tagged myristoylated phosphatase domain of PTPRJ or the inactive mutant (PTPRJ-D/A). Transfected cells were infected with Opa_{52}-expressing (Opa_{52}) or Opa-negative (Opa-) *N. gonorrhoeae* (MOI of 30) for 15 min or remained uninfected. Subsequently, WCL were prepared, and expression of PTPRJ-mCherry (*upper panel*) and CEACAM3-GFP or GFP (*middle panel*) was confirmed by immunoblotting with appropriate antibodies. Lysates were probed with α-tubulin antibodies to confirm equal loading (lower panel). *B,* lysates from (*A*) were incubated with GFP-binding nanobodies and GFP or CEACAM3-GFP was immunoprecipitated. Tyrosine phosphorylation of CEACAM3 in the precipitates was analyzed by Western blotting with α-phospho-tyrosine (pTyr) antibody (*upper panel*). Equal immunoprecipitation from the samples was verified by probing with α-CEACAM3 (*middle panel*) and α-GFP antibodies (*lower panel*). *C,* c-Src was immunoprecipitated from cell lysates as in (*A*). The tyrosine phosphorylation status of c-Src was determined by Western blotting with antibodies directed against phosphorylated Y418 (pY418; *upper panel*; corresponds to pY419 in human c-Src) or pY527 (middle panel; corresponds to pY530 in human c-Src). Probing with α-c-Src antibodies confirmed equal loading (*lower panel*). *D,* c-Src was immunoprecipitated from lysates of serum-starved (-) or serum-stimulated (+) murine embryonic fibroblasts, and the samples were probed as in C). *E,* the tyrosine phosphorylation status of $p130^{Cas}$ was determined by Western blotting with antibodies directed against phosphorylated Y410 of $p130^{Cas}$ (pY410; *upper panel*), while probing with α-$p130^{Cas}$ antibody (*middle panel*) and α-tubulin (*lower panel*) confirmed equal loading. CEACAM3, carcinoembryonic antigen-related cell adhesion molecule 3; PTPR, receptor-type protein tyrosine phosphatase; WCL, whole cell lysate.

(Fig. 3*D*). In agreement with a negligible effect on c-Src phosphorylation and activity, the expression of myr-PTPRJ did also not abrogate the increased tyrosine phosphorylation of the c-Src substrate $p130^{Cas}$ (Fig. 3*E*). These data demonstrated that the presence of active PTPRJ selectively altered the phosphorylation state of CEACAM3, while PTPRJ did not influence c-Src tyrosine phosphorylation or c-Src activity, suggesting that PTPRJ might directly act on CEACAM3.

Recombinant PTPRJ dephosphorylates the CEACAM3 tyrosine residues Y230 and Y241

While overexpression of PTPRJ resulted in reduced tyrosine phosphorylation of CEACAM3, this might be an indirect effect mediated by PTPRJ acting on another protein phosphatase or protein kinase. Therefore, we tested the ability of PTPRJ to directly dephosphorylate tyrosine residues within the CEACAM3 ITAM-like motif. To this end, we recombinantly expressed and purified the phosphatase domains of wildtype

human PTPRJ and of the inactive PTPRJ-D/A mutant (PTPRJ-D/A) in the form of His-tagged proteins in *E. coli* (Fig. 4*A*). The enzymatic activity of the recombinant proteins was confirmed by *in vitro* phosphatase assay with the generic substrate 4-methylumbelliferyl phosphate (4-MUP). Importantly, wildtype PTPRJ dephosphorylated 4-MUP, while the PTPRJ D/A mutant did not show catalytic activity (Fig. 4*B*). Next, we incubated the recombinant phosphatase with synthetic phospho-peptides spanning the CEACAM3 ITAM-like motif and bearing a phospho-tyrosine residue at either position Y230 or Y241 (Fig. 4*C*). While wildtype PTPRJ readily dephosphorylated each phospho-tyrosine–containing peptide in a dose-dependent manner, PTPRJ-D/A showed no activity (Fig. 4*D*). Phosphate release from both tyrosine residues by

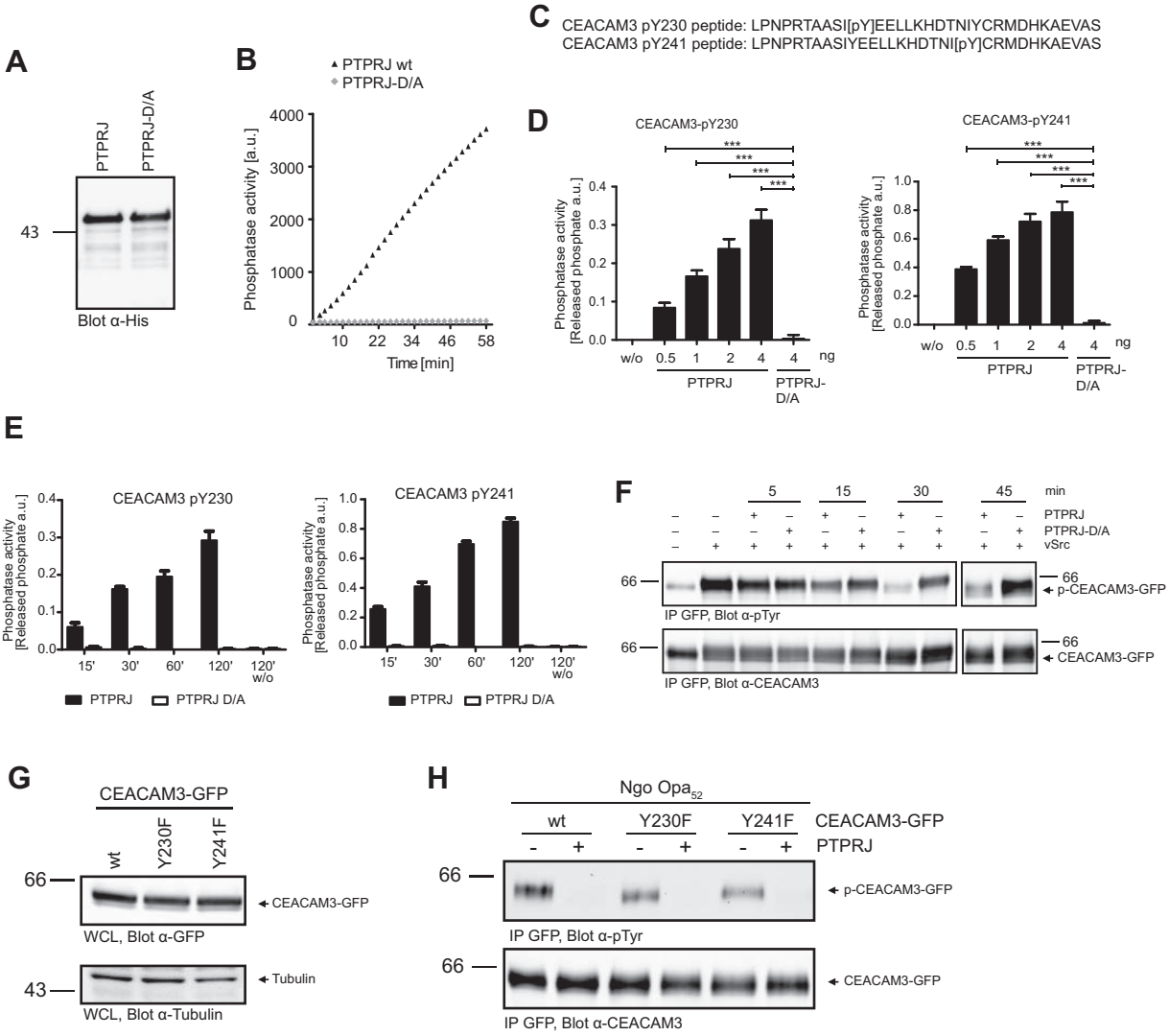

Figure 4. Recombinant PTPRJ dephosphorylates the CEACAM3 tyrosine residues Y230 and Y241. *A,* recombinant phosphatase domains of His-PTPRJ and His-PTPRJ-D/A were expressed *in E. coli*, purified, and analyzed by Western blotting using an α-His antibody. *B,* 12.5 ng recombinant PTPRJ or PTPRJ-D/A phosphatase domains were incubated with 500 μM of 4-MUP. Shown is the increase in 4-MU fluorescence of a representative experiment over a 60-min period. *C,* synthetic phospho-peptides spanning the carboxy-terminus of CEACAM3. Either tyrosine residue 230 (pY230) or 241 (pY241) of the ITAM-like sequence is phosphorylated. *D,* CEACAM3 phospho-peptides were incubated at 30 °C without phosphatases (w/o) or with the indicated amounts of recombinant PTPRJ or PTPRJ-D/A phosphatase domains. Released phosphate was determined by malachite green. Background values (buffer plus malachite green) were subtracted. Bars represent mean ± SD of three independent experiments. Statistically significant differences were determined by one-way ANOVA followed by Dunnett's posttest. $^{**}p < 0.01$; $^{***}p < 0.001$. *E,* CEACAM3 phospho-peptides were incubated with or without 1 ng of recombinant PTPRJ or PTPRJ-D/A for the indicated time at 30 °C. Released phosphate was determined as in (*D*). Bars show mean ± SD from three technical replicates. *F,* CEACAM3-GFP was co-expressed or not with the active tyrosine kinase v-Src in 293T cells. CEACAM3-GFP immunoprecipitates were incubated with 200 ng recombinant His-PTPRJ or His-PTPRJ-D/A phosphatase domains for the indicated times at 30 °C. CEACAM3 tyrosine phosphorylation was monitored by Western blot analysis using α-phospho-tyrosine antibodies (*upper panels*). Probing of the membrane with α-CEACAM3 antibodies (*lower panels*) confirmed equal precipitation of CEACAM3-GFP. *G,* 293T cells were transfected to express CEACAM3-GFP wildtype, CEACAM3-GFP Y230F, or CEACAM3-GFP Y241F. Immunoblotting with α-GFP antibodies (*upper panel*) and α-tubulin (*lower panel*) confirmed equal expression of CEACAM3 variants as well as equal loading of the samples. *H,* 293T cells transfected as in (*G*) were infected at an MOI of 30 with Opa_{52}-expressing (Opa_{52}) *N. gonorrhoeae* for 15 min. Cells were lysed, and wildtype CEACAM3-GFP and CEACAM3 mutants were immunoprecipitated. Immunoprecipitates were incubated for 45 min at 30 °C with or without recombinant PTPRJ phosphatase (400 ng). Samples were examined by Western blot analysis with α-phospho-tyrosine antibodies (*upper panel*). Equivalent amounts of immunoprecipitated CEACAM3 were verified by probing with α-CEACAM3 (*lower panel*). 4-MUP, 4-methylumbelliferyl phosphate; CEACAM3, carcinoembryonic antigen-related cell adhesion molecule 3; ITAM, immunoreceptor tyrosine-based activation motif; PTPR, receptor-type protein tyrosine phosphatase.

PTPRJ was linear over the course of 60 min and occurred with comparable efficiency (Fig. 4*E*). Taken together, these results show that recombinant PTPRJ is able to directly catalyze the hydrolysis of both phosphorylated tyrosine residues of the CEACAM3 ITAM-like motif *in vitro*.

To investigate, if PTPRJ also dephosphorylates both residues in the context of the native CEACAM3 protein, we expressed GFP-tagged CEACAM3 in 293T cells in the presence or absence v-Src. As reported previously, co-expression of v-Src leads to strong, constitutive tyrosine phosphorylation of the CEACAM3 ITAM-like motif (14, 19, 34) (Fig. 4*F*). Upon precipitation of CEACAM3-GFP from whole-cell lysates, the protein was incubated with recombinant PTPRJ wildtype or the inactive D/A mutant for 5 to 45 min (Fig. 4*F*). Clearly, incubation of tyrosine phosphorylated CEACAM3 with the wildtype phosphatase led to an almost complete dephosphorylation in the course of 30 to 45 min, while PTPRJ-D/A did not affect the phosphorylation state of CEACAM3 (Fig. 4*F*). Moreover, we transfected 293T cells with either CEACAM3 wildtype or CEACAM3 mutants with a single phosphorylatable tyrosine residue in the ITAM-like motif (CEACAM3 Y230F and CEACAM3 Y241F). All constructs were expressed at similar levels (Fig. 4*G*). Following infection with CEACAM3-binding *N. gonorrhoeae*, CEACAM3 proteins were precipitated from cells and incubated or not with recombinant PTPRJ for 45 min. As expected, CEACAM3 Y230F and CEACAM3 Y241F showed reduced tyrosine phosphorylation levels compared to wildtype CEACAM3 (Fig. 4*H*). However, upon incubation with recombinant PTPRJ all proteins were completely dephosphorylated (Fig. 4*H*). These findings confirm the ability of PTPRJ to directly dephosphorylate both tyrosine residues embedded within the CEACAM3 ITAM-like motif, suggesting that PTPRJ can limit CEACAM3-initiated, tyrosine phosphorylation-dependent processes such as phagocytosis of human restricted pathogens.

PTPRJ deletion in human phagocytes results in elevated phagocytosis

As CEACAM3 is expressed exclusively by human granulocytes, we wondered about the functional interaction of this phagocytic receptor and PTPRJ in myeloid cells. Accordingly, we generated PTPRJ-deficient clonal HL-60 lines by lentiviral transduction of HL60 CEACAM3-mKate2 cells with Cas9 and sgRNAs targeting PTPRJ (HL60-CEACAM3-mKate2 sgPTPRJ clone 6 and clone 12). As a control, HL60-CEACAM3-mKate2 cells were transduced with Cas9 and sgRNA targeting Cerulean (HL60-CEACAM3-mKate2 sgCer). Western blotting, flow cytometry, and immunofluorescence staining confirmed that the derived HL60-CEACAM3-mKate2 sgPTPRJ cells completely lacked PTPRJ expression (Figs. 5, *A* and *B* and S1). Expression of PTPRC, a related receptor protein tyrosine phosphatase expressed in immune cells, was not affected (Fig. 5*C*), and HL60-CEACAM3-mKate sgCer and HL60-CEACAM3-mKate sgPTPRJ clone 6 cells showed equivalent surface expression of CEACAM3 (Fig. 5*D*). In line with the observations of the initial CRISPR/Cas9 screen, the clonal PTPRJ-deficient HL60-CEACAM3 cells exhibited increased CEACAM3-mediated uptake of Opa_{52}-expressing *N. gonorrhoeae* (Fig. 5, *E* and *F*). Importantly, increased uptake by PTPRJ-deficient cells was not seen for nonopaque, non-CEACAM–binding gonococci, demonstrating that enhanced phagocytosis depended on Opa-protein-CEACAM3-interaction (Fig. 5, *E* and *F*). Together, these findings corroborate the idea that PTPRJ action limits CEACAM3-mediated phagocytosis by human myeloid cells.

PTPRJ deletion in human phagocytes leads to a gain-of-function phenotype

As CEACAM3-initiated responses are accompanied by phenotypic changes of the phagocytes, such as remodeling of the actin cytoskeleton and induction of prominent cell protrusions, we investigated infected samples by scanning electron microscopy (SEM). Clearly, uninfected HL60-CEACAM3-mKate sgCer and HL60-CEACAM3-mKate sgPTPRJ showed small filopodia-like protrusions throughout the cell body (Fig. 6*A*). Upon infection with CEACAM-binding gonococci, lamellipodia with a length of 1 to 2 μm emerged locally in HL-60 CEACAM3-mKate sgCer cells (Fig. 6*A*). However, lamellipodia formation by infected PTPRJ-deficient HL-60 cells was markedly magnified with wider and larger (>2 μm) lamellipodia formed (Fig. 6*A*). Based on 10 distinct SEM images of each sample, we estimated the area covered by individual lamellipodia. While lamellipodia in wildtype cells extended on average over ∼7 μm^2 in response to infection with CEACAM-binding bacteria, in PTPRJ knock-out cells this area was doubled (Fig. 6*B*). Together, these findings illustrate that PTPRJ is a negative regulator of CEACAM3-initiated phagocyte functions and that PTPRJ action on CEACAM3 prevents exaggerated phagocyte responses.

Discussion

CEACAM3 is a specialized phagocytic receptor, enabling primate granulocytes to detect and eliminate a restricted set of host-adapted bacterial pathogens (5). CEACAM3 downstream signaling is initiated by tyrosine phosphorylation of a characteristic sequence motif in the cytoplasmic domain of this receptor. Here, we reveal that CEACAM3 signaling is controlled by the receptor-type tyrosine phosphatase PTPRJ (also known as CD148 and DEP-1). PTPRJ activity is directed toward the phosphorylated tyrosine residues of CEACAM3, thereby constraining CEACAM3-initiated cellular responses.

In this regard, PTPRJ appears as the second negative regulator of CEACAM3 signaling, which acts directly on the receptor protein. Grb14, a SH2 domain-containing adaptor protein, has previously been shown to associate with the phosphorylated tyrosine residue Y230 of CEACAM3 and thereby prohibits access of functionally important binding partners (34). Indeed, pY230 is the major binding site of SH2 domains encoded by Src family kinases, the GEF Vav, and the adapter protein Nck, which together orchestrate the

cytoskeletal rearrangements required for efficient phagocytosis (17). By competitive binding to pY230, Grb14 interferes with CEACAM3 downstream signaling and reduces bacterial uptake. In a similar manner, PTPRJ achieves a comparable outcome, by slightly different means; this enzyme readily dephosphorylates the tyrosine residues embedded in the ITAM-like motif, thereby completely abrogating the phosphorylation-dependent, SH2-domain–mediated binding by multiple interaction partners.

A direct action of PTPRJ on CEACAM3 is supported by the *in vitro* dephosphorylation of phospho-peptides derived from the CEACAM3 ITAM-like motif by recombinant PTPRJ. Moreover, the recuded CEACAM3 phosphorylation observed in PTPRJ-overexpressing cells, which do not show changes in the phosphorylation pattern of Src family kinases, is further strong evidence that CEACAM3 is a direct substrate of PTPRJ. The lack of an effect of PTPRJ on Src family kinases might appear surprising given the known positive role of PTPRJ for Src PTK activation in platelets, but this might be different in human myeloid cells, where absence of PTPRJ has been linked to increased activity of receptor protein tyrosine kinases (35) and where the activation of Src family kinases can be mediated by distinct PTPRs, such as PTPRC (CD45) (24, 36).

Similar to other PTPRs, PTPRJ is characterized by the possession of a large, multidomain extracellular part. This spacious extracellular part of the enzyme is functionally relevant during phagocytosis, as it leads to the displacement of PTPRJ by a surface-bound particle (26). A similar situation can be envisioned in the case of gonococci associating with

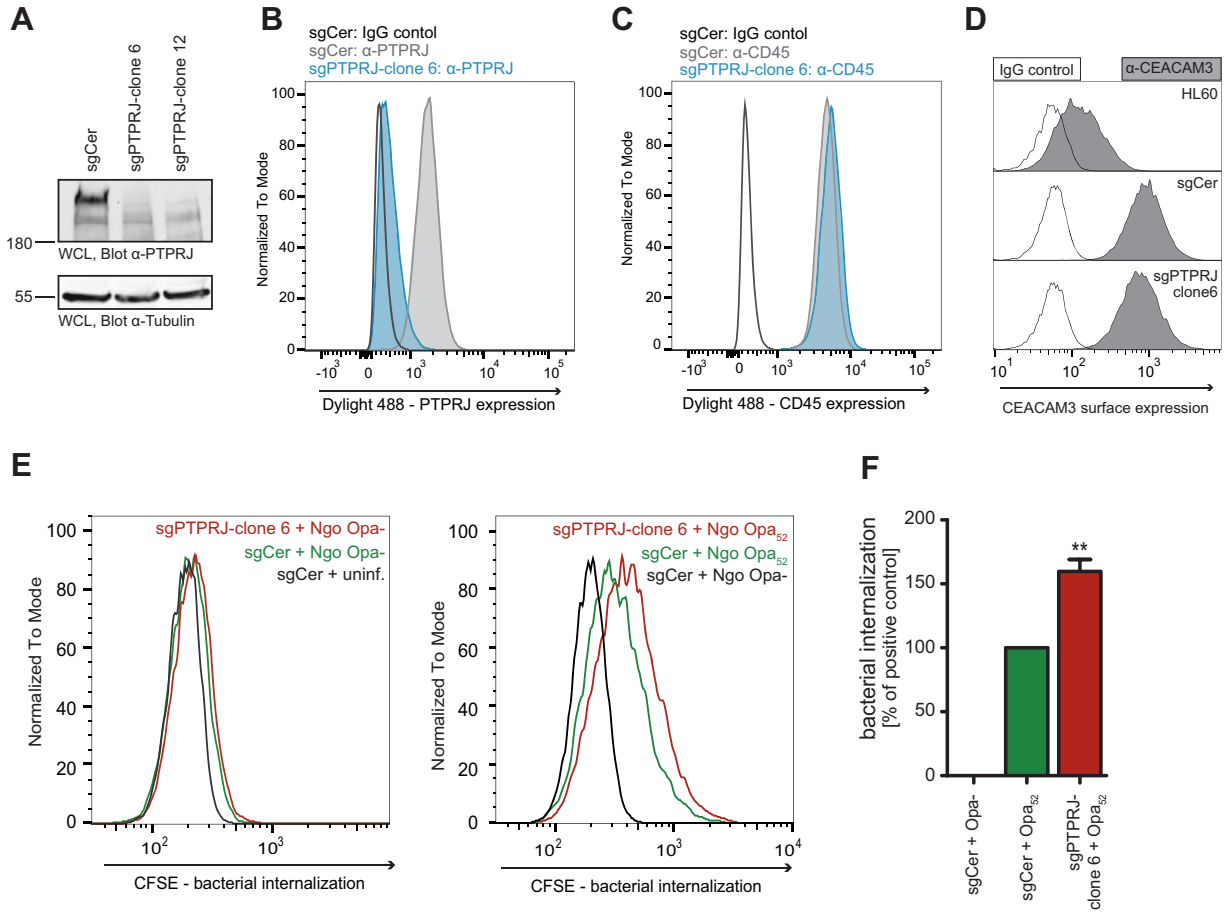

Figure 5. PTPRJ deletion in human phagocytes results in elevated phagocytosis. *A,* HL60 CEACAM3-mKate Cerulean cells were treated with sgRNAs against cerulean (HL60 CEACAM3-mKate control) or a combination of sgRNAs against cerulean and PTPRJ (HL60 CEACAM3-mKate sgPTPRJ). PTPRJ expression in whole cell lysates (WCLs) of the indicated clonal cell lines was analyzed by Western blotting with α-PTPRJ antibodies (*upper panel*). Equal loading was confirmed by probing with α-tubulin (*lower panel*). *B,* PTPRJ expression in HL60 CEACAM3-mKate control (*gray filled curve*) or HL60 CEACAM3-mKate sgPTPRJ clone 6 cells (*blue filled curve*) was analyzed by surface staining with α-PTPRJ antibodies and flow cytometry. A sample of HL60 CEACAM3-mKate control cells was also stained with an isotype-matched primary control antibody (IgG control, *open curve*). *C,* PTPRC expression in cells as in (*B*) was analyzed by surface staining with α-PTPRC antibodies and flow cytometry. A sample of HL60 CEACAM3-mKate control cells was also stained with an isotype-matched primary control antibody (IgG control, open curve). *D,* CEACAM3 expression in HL60 cells, HL60 CEACAM3-mKate control cells, and HL60 CEACAM3-mKate sgPTPRJ clone 6 cells was analyzed by staining with α-CEACAM3 antibodies and flow cytometry (*gray filled curve*). Each cell line was also stained with an isotype-matched primary control antibody (IgG control, open curve). *E,* HL60-CEACAM3-mKate sgPTPRJ cells or HL60 CEACAM3-mKate control cells were infected for 10 min at an MOI of 10 with CFSE-labeled *N. gonorrhoeae* expressing either Opa_{52} (Ngo Opa_{52}) or no Opa-adhesin (Ngo Opa-). After quenching the fluorescence of extracellular bacteria with trypan blue, the CSFE signal of internalized bacteria was measured by flow cytometry. Shown is a representative experiment. *F,* quantification of bacterial internalization assays performed as in (*E*). Bars represent mean fluorescent intensities (MFIs) ± SEM from five independent experiments and are normalized to the CFSE fluorescence detected upon infection of HL60 CEACAM3-mKate control cells with Opa_{52}-expressing *N. gonorrhoeae*. Statistically significant increases in bacterial internalization were determined by Student's *t* test and indicated by *asterisks*; $^{**}p < 0.01$. CEACAM3, carcinoembryonic antigen-related cell adhesion molecule 3; CFSE, carboxyfluorescein succinimidyl ester; PTPR, receptor-type protein tyrosine phosphatase.

CEACAM3. The tight binding of the bacteria to CEACAM3 leads to a close apposition of the particle and the phagocyte membrane as observed by SEM (7, 16). Accordingly, the steric hindrance of the large extracellular domain of PTPRJ would result in a lateral displacement of the protein phosphatase away from the clustered, pathogen-bound receptor. As a consequence of this microscale spatial separation, the local absence of PTPRJ could give way to elevated tyrosine phosphorylation of the CEACAM3 ITAM-like motif, whenever the receptor is engaged by a particle. In line with this elegant concept of a phagocytic synapse formation (26), truncation of the large extracellular domain of PTPRJ results in a constitutive-active form of the protein phosphatase, which cannot get displaced by a bound particle and therefore diminishes CEACAM3-mediated phagocytosis. Another mode of PTPRJ regulation, which depends on the generation of reactive oxygen by the NADPH oxidase has been reported from human acute myeloid leukemia cells (37). As CEACAM3-initiated signals trigger strong GTP-loading of Rac and NADPH oxidase assembly, PTPRJ could also become enzymatically silenced *via* reactive oxygen species acting on critical cysteine residues in the phosphatase domain (38). In this way, NADPH oxidase action might generate a positive feedback loop to promote sustained tyrosine phosphorylation of CEACAM3 by dampening PTPRJ activity.

Together, our results indicate that human granulocytes possess multiple, independent means of regulating the phosphorylation state of the CEACAM3 ITAM-like motif. This finding implies that tight control of this receptor is needed to prevent unintended activity. Indeed, by triggering the release of proinflammatory cytokines and inducing massive stimulation of reactive oxygen production (7, 19, 39, 40), uncontrolled CEACAM3 signaling has the potential to cause severe cell and tissue damage. On the other hand, the action of this granulocyte receptor can protect our body from harmful microbes suggesting that the negative regulation by PTPRJ or Grb14 has to be finely tuned to allow maximum effectivity of CEACAM3 at infection sites.

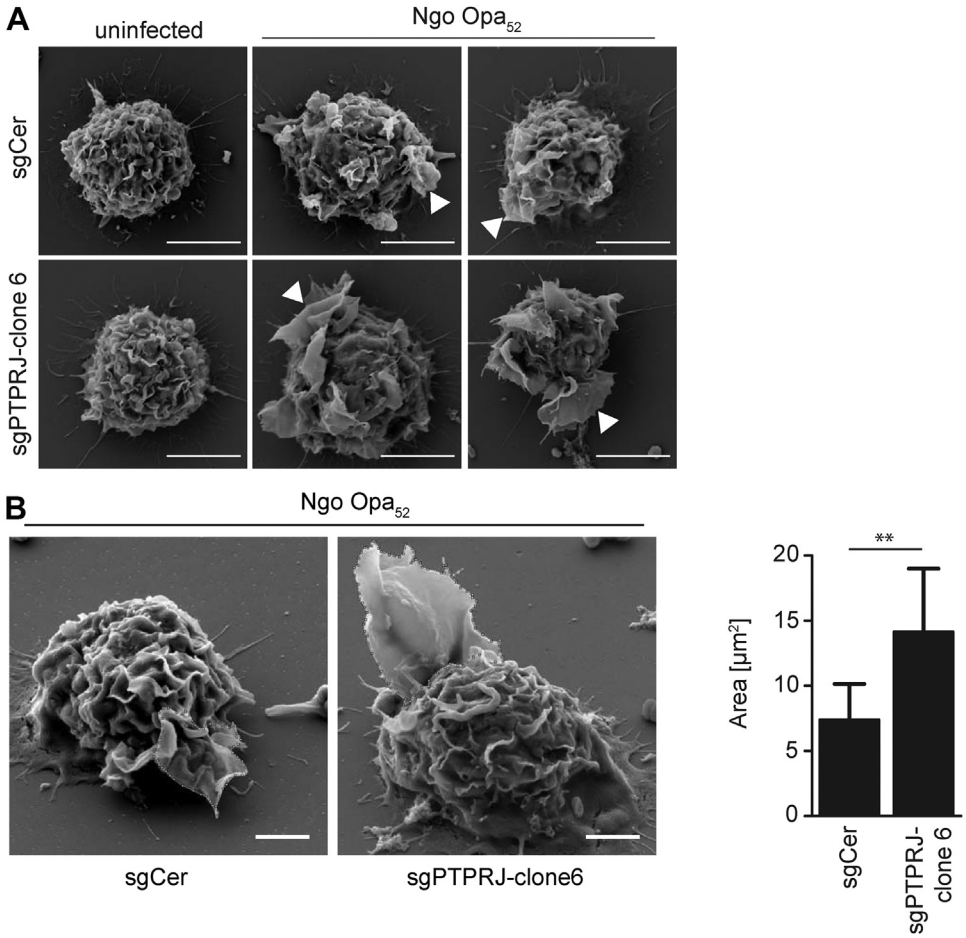

Figure 6. Deletion of PTPRJ in human phagocytes results in a gain-of-function phenotype. *A,* HL60 CEACAM3-mKate2 PTPRJ-cells (PTPRJ-) and HL60-CEACAM3-mKate2 control cells (sgCer) were left uninfected or were infected with Opa_{52}-expressing *N. gonorrhoeae* for 30 min (MOI 30). Cells were fixed and analyzed by scanning electron microscopy. *Arrowheads* point to lamellipodia involved in phagocytosis. Scale bars represent 5 µm. *B,* in samples from (*A*), the extension of bacteria-induced lamellipodia was determined by manual determination of the circumference and calculation of the area in NIH ImageJ as in the depicted examples. Scale bars represent 2 µm. The *broken line* indicates the circumference of the lamellipodia. Bars in the right panel represent mean lamellipodial area in μm^2 ± SD of 10 individual cells for each condition. Statistically significant differences were determined by two-sided Student's *t* test and indicated by *asterisks*. $^{**}p < 0.01$. CEACAM3, carcinoembryonic antigen-related cell adhesion molecule 3; PTPR, receptor-type protein tyrosine phosphatase.

Experimental procedures

Antibodies

The following primary and secondary antibodies were used: primary antibodies: α-CEACAM3 (mouse monoclonal anti-CEACAM3/CEACAM5, 308/3–3 from ImmunoTools, WB: 1:2000, FC: 1:200); α-GFP (mouse monoclonal, JL8 from Clontech, WB: 1:5000); α-6x His (mouse monoclonal, H8 from Thermo Scientific, WB: 1:1000); α-Opa (mouse monoclonal, 4B12/C11, Developmental Studies Hybridoma Bank, University of Iowa, USA, a generous gift of M. Achtman (41), WB: 1:2000); α-PTPRC (mouse monoclonal, 35-Z6 from Santa Cruz, FC: 1:200); α-PTPRJ (DEP-1) (mouse monoclonal, 143–41 from Santa Cruz, WB: 1:1000, FC: 1:200, IF: 1:100); α-RFP (used to detect mCherry, mouse monoclonal, clone 6G6 from Chromo Tek, WB: 1:2000); α-cSrc (rabbit polyclonal, SRC2 (sc-18) from Santa Cruz, WB 1:1000); α-phospho-Src (pY418) (rabbit polyclonal Cat.# 44660G from Invitrogen, WB: 1:500); α-phospho-Src (pTyr527) (rabbit polyclonal, #2105 from Cell Signaling, WB 1:500); α-$p130^{Cas}$ (mouse monoclonal, P27820 from Transduction Laboratories, WB 1:1000); α-phospho-$p130^{Cas}$ pY410 (rabbit polyclonal, #4011 from Cell Signaling, WB 1:500); α-Tubulin (mouse monoclonal, clone E7 from Developmental Studies Hybridoma Bank, University of Iowa, USA, WB: 1:1000); α-phospho-tyrosine (mouse monoclonal, PY72 from Upstate Biotechnology, WB 1:1000); α-Vinculin (mouse monoclonal, clone hVIN-1 from Sigma-Aldrich, WB: 1:1000); secondary antibodies: horseradish peroxidase (HRP)-conjugated goat anti-mouse (Jackson ImmunoResearch Inc., WB: 1:10.000), horseradish peroxidase (HRP)-conjugated goat anti-rabbit (Jackson ImmunoResearch Inc., WB: 1:5000) and Alexa Fluor 488-conjugated AffiniPure goat anti-mouse (Jackson ImmunoResearch Inc., IF: 1:200, FC: 1:200).

Cell culture and transient transfection

Human embryonic kidney 293T cells (293T cells) (DSMZ) were cultured in Dulbecco's modified Eagle's medium supplemented with 10% calf serum. 293T cells seeded the previous day at approximately 25% confluency were transfected with 5 μg of plasmid DNA using calcium phosphate precipitation. Samples were treated with 25 μM chloroquine for 6 to 8 h, before the culture medium was replaced with 10 ml of fresh Dulbecco's modified Eagle's medium containing 10% calf serum. Cells were lysed 48 h after transfection. Murine embryonic fibroblasts (42) were cultured in DMEM supplemented with 10% fetal calf serum (FCS), nonessential amino acids, and sodium pyruvate.

HL60 cells (ATCC) were cultured in RPMI 1640 medium supplemented with 10% FCS. 293T, murine embryonic fibroblasts, and HL60 cells were maintained at 37 °C and 5% CO_2 and were splitted every 2 to 3 days.

Bacterial strains and growth conditions

N. gonorrhoeae MS11-B2.1 strains (nonpiliated *N.gonorrhoeae* Opa_{52} (N309) and nonpiliated *N.gonorrhoeae* MS11-B2.1 Opa^- (N302)) (43) were grown on GC agar plates supplemented with vitamins, chloramphenicol (10 μg/ml), and erythromycin (7 μg/ml). Bacteria were cultured at 37 °C and 5% CO_2 and were passaged daily.

Recombinant DNA

The lentiviral pLL3.7-Cerulean-vector was generated by replacing the GFP-cDNA of the pLL3.7 vector (a kind gift from Luk Parijs; Addgene #11795) with the Cerulean-cDNA from the mCerulean C1 plasmid (a kind gift from Steven Vogel; Addgene #27796). This was achieved by digestion of both plasmids with the restriction enzymes AgeI and BsrGI followed by ligation of the Cerulean-coding sequence into the pLL3.7-backbone. The Cerulean-targeting CRISPR plasmid pLentiCRISPRv2-sgRNACerulean, which was used to generate HL60-CEACAM3-mKate control cells, is based on the pLentiCRISPRv2 vector (a kind gift from Feng Zhang; Addgene #52961, (44)) and has been described before (42). To derive the pLentiCRISPRv2-sgCerulean-w/o-Cas9 vector, pLentiCRISPRv2-sgRNACerulean was digested with BsmBI and a linker oligo was inserted (using the annealed sense oligo 5′-CACCGGAGACGGATGGGCCCAATTCGAATACACGTGGTTGATTTAAATGGGCCCCGTCTCC-3′ and antisense oligo 5′-AAACGGAGACGGGGCCCATTTAAATCAACCACGTGTATTCGAATTGGGCCCATCCGTCTCC-3′). Next, the Cas9 coding sequence was removed from the backbone by digestion with AgeI and BamHI followed by religation with an annealed stuffer (5′-CCGGTTCTAGAGCGCTGCCACCATGG-3′ and 5′-GATCCCATGGTGGCAGCGCTCTAGAA-3′).

Lentiviral sgPTPRx sequence-containing plasmids were generated using plentiCRISPRv2, which was digested with BsmBI and then ligated with the corresponding BsmBI overhang-containing PTPRx-sgRNA oligopair. The sgRNA sequences used for targeting specific PTPRs are listed in Table 1.

Expression vectors encoding the myristoylated phosphatase domains were constructed from the full-length cDNA of PTPRJ (generous gift from I. Royale, University of Montreal, Canada (45)), PTPRS (Harvard Medical School, plasmid collection # HsCD00341547), PTPRG (Arizona State University, DNASU Plasmid Repository # HsCD00829408), and PTPRF (Arizona State University, DNASU Plasmid Repository # HsCD00021632). The phosphatase domain encoding cDNAs were amplified by PCR using primers that introduced ligation-independent cloning (LIC) overhangs and an N-terminal myristoylation site (myr-PTPRF: 5′-ACTCCTCCCCCGCCATGGGATGTATAAAATCAAAAGGGAAAGACAAAAGGAAAAGGACCCACTC-3′ and 5′-CCCCACTAACCCGCGTTGCATAGTGGTCAAAGC-3′; myr-PTPRG: 5′-ACTCCTCCCCCGCCATGGGATGTATAAAATCAAAAGGGAAAGACAGAGGGTGTAACAAAATAAAGTCC-3′ and 5′-CCCCACTAACCCGCACTAGGGACTCCATGCTCTCAGC-3′; myr-PTPRJ: 5′-ACTCCTCCCCCGCCATGGGATGTATAAAATCAAAAGGGAAAGACAGAAAGAAGAGGAAAGATGC-3′ and 5′-CCCCACTAACCCGGGCGATGTAACCATTGG-3′; myr-PTPRS: 5′-ACTCCTCCCCCGCCATGGGATGTATAAAATCAAAAGGGAAAGACCTGCTCTACAAG

Table 1
Oligonucleotides (sgRNAs) used for the CRISPR/Cas9-mediated knockout of receptor-type protein tyrosine phosphatases (PTPRs)

	Forward (5′ – 3′)	Reverse (5′ – 3′)
Targeted gene	BsmBI-overhang, sense sgRNA	BsmBI-overhang, antisense sgRNA
PTPR**A**	CACCGCTGTTCTGGCATCCGTGAAC	AAACGTTCACGGATGCCAGAACAGC
PTPR**B**	CACCGTGTGGTGTTGTCTATCCGAA	AAACTTCGGATAGACAACACCACAC
PTPR**C**	CACCGTTACCACATGTTGGCTTAGA	AAACTCTAAGCCAACATGTGGTAAC
PTPR**D**	CACCGTCGAACTCAACATTCGTGCC	AAACGGCACGAATGTTGAGTTCGAC
PTPR**E**	CACCGCACTCCGAAGTCGGGCCAGC	AAACGCTGGCCCGACTTCGGAGTGC
PTPR**F**	CACCGTCATCTCGCTGCACCCGCAA	AAACTTGCGGGTGCAGCGAGATGAC
PTPR**G**	CACCGCGGGGAAGCACACGACATAA	AAACTTATGTCGTGTGCTTCCCCGC
PTPR**H**	CACCGAACAGCCACCAACGTCACCG	AAACCGGTGACGTTGGTGGCTGTTC
PTPR**J**	CACCGCAGGCTCTAACCCGACAAGC	AAACGCTTGTCGGGTTAGAGCCTGC
PTPR**K**	CACCGAGGGGCCTGTGATTACCACC	AAACGGTGGTAATCACAGGCCCCTC
PTPR**M**	CACCGGATGAGCCGTATAGCACATG	AAACCATGTGCTATACGGCTCATCC
PTPR**N1**	CACCGCAGGCTGTCTATTTGACCGC	AAACGCGGTCAAATAGACAGCCTGC
PTPR**N2**	CACCGGGCGTCGGAGGGCGTTGGCC	AAACGGCCAACGCCCTCCGACGCCC
PTPR**O**	CACCGTAGTAATATCACCTTTCAGC	AAACGCTGAAAGGTGATATTACTAC
PTPR**Q**	CACCGGCTCATCACAGTGGCAGACC	AAACGGTCTGCCACTGTGATGAGCC
PTPR**R**	CACCGTCTCCCATAAACCGAAAAAC	AAACGTTTTTCGGTTTATGGGAGAC
PTPR**S**	CACCGGTTCCCTACCTCGCACGTAG	AAACCTACGTGCGAGGTAGGGAACC
PTPR**T**	CACCGCCTGGGAGCAGATTAACACA	AAACTGTGTTAATCTGCTCCCAGGC
PTPR**U**	CACCGCGTTGACCTCCACGTCGCCC	AAACGGGCGACGTGGAGGTCAACGC
PTPR**Z1**	CACCGAACACATTCATTCATAACAC	AAACGTGTTATGAATGAATGTGTTC

AACAAACC-3′ and 5′-CCCCACTAACCCGGGTTGCATA GTGGTCAAAGC-3′). The PTPRJ-D1205A (PTPRJ-D/A) mutation was introduced by PCR with overlapping extension (SOEing) using the LIC-based myr-PTPRJ forward and reverse primer together with a mutation introducing complementary forward and reverse primer (5′-CCATTTCACC TCCTGGCCAGCCCACGGTGTTCCCGACACC-3′ and 5′-GGGGGTGTCGGGAACCGTGGCTGGCCAGGAGGTGAAA TGG-3′). Subsequently, the PCR products were inserted into the pDNR dual-LIC vector (5). From the resulting pDNRdual-LIC-myr-PTPRx vectors, the inserts were transferred by Cre-based recombination into mammalian expression vectors containing mScarlet (pLPS3′-mScarlet) or mCherry (pLPS3′-mCherry). The resulting expression constructs encode the respective myristoylated phosphatase domain with a fluorescent protein fused to the carboxy-terminus. pLPS3′-mScarlet and pLPS3′-mCherry were created by replacing the EGFP-encoding cDNA of the pLPS3′-EGFP acceptor vector (Clontech) with the cDNA of mScarlet derived from vector pmScarlet-C1 (kind gift from Dorus Gadella; Addgene #85042) or with the cDNA of mCherry derived from vector pRSET-B mCherry (kind gift from Kalina Hristova; Addgene #108857), respectively.

Cloning and expression of the recombinant PTPRJ phosphatase domain

For bacterial expression of the 6xHis-Sumo-tagged PTPRJ and PTPRJ-D/A phosphatase domains, the cDNAs encoding the phosphatase domain were amplified from the pLPS3′-mCherry-myr-PTPRJ and pLPS3′-mCherry-myr-PTPRJ-D/A constructs described above using primers PTPRJ-PTP_SacI_for (5′-ATAGAGCTCAGGGTTCGCAGAGGAATACG-3′) and PTPRJ-PTP_NotI_rev (5′-ATAGCGGCCGCTCATCTGA-CAATATCCAAAACACACTG-3′). The PCR products were digested with SacI/NotI and cloned into pET24a-His-Sumo (46). Phosphatase domains were expressed in *E. coli* BL21(DE3) upon induction with IPTG, purified using a His-FF column (GE Healthcare), and dialyzed with 50 mM Tris, pH 7.5, 150 mM NaCl, and 10% glycerol.

Whole cell lysates and Western blotting

Cells were lysed in RIPA buffer (0.1% w/v SDS, 1% sodium deoxycholic acid, 1% Triton X-100, 50 mM Hepes, 150 mM NaCl, 10% glycerol, 1.5 mM $MgCl_2$, 1 mM EGTA, 10 mM sodium pyrophosphate, and 100 mM NaF) or NP40 lysis buffer (50 mM Tris-HCl, pH7.4, 150 mM NaCl, 1% NP40, 1 mM EDTA, 50 mM NaF) in the presence of protease inhibitors, 1 mM sodium orthovanadate, and 10 mM of para-nitrophenol phosphate. After centrifugation at 13,000 rpm and 4 °C for 30 min, cleared whole cell lysates were taken up in SDS buffer and boiled at 95 °C for 5 to 10 min. Proteins were separated by SDS-PAGE and transferred to polyvinylidene difluoride membranes. Subsequently, membranes were blocked in blocking buffer (50 mM Tris-HCl pH 7.5, 150 mM NaCl, 0.05% Tween 20, 2% BSA) for 1 h at RT and then incubated with primary antibodies (diluted in blocking buffer) overnight at 4 °C. The next day, membranes were washed three times with TBS-T (50 mM Tris-HCl pH 7.5, 150 mM NaCl, 0.05% Tween 20) and incubated with the HRP-conjugated secondary antibody (in TBS-T) for 1 h at RT, before ECL detection on a Chemidoc Touch Imaging System (Bio-Rad).

Lentivirus production in 293T cells and transduction of HL60 cells

Lentiviral particles were produced by transient transfection of 293T cells with the plasmids pMD2.G (Addgene #12259) (3.5 μg), psPAX2 (Addgene #12260) (5 μg), and the respective lentiviral vector (6.5 μg). Three days after transfection, the virus-containing supernatant was collected, sterile filtered (pore size 0.45 μm), and added to the recipient cells, which also received 8 μg/ml hexadimethrine bromide. Virus-infected cultures were centrifuged at 800*g* for 1 h to spin the viral particles onto the cells (spinfection). First, HL60-CEACAM3-mKate2-expressing cells (5) were transduced with lentiviral particles encoding pLL3.7-Cerulean to obtain a stable Cerulean expressing HL-60-CEACAM3-mKate2 cell line (HL60-CEACAM3-mKate2-Cerulean cells). Next, HL60-CEACAM3-

mKate2-Cerulean cells were simultaneously transduced with two distinct lentiviral particles, one produced using a defined pLentiCRISPRv2-sgPTPRx construct and the other using the pLentiCRISPRv2-sgCerulean-w/o-Cas9 vector. HL60-CEACAM3-mKate2 control cells were transduced with pLentiCRISPRv2-sgRNACerulean encoding lentiviral particles. For the genetic screen, transduced HL-60 populations were employed 1 week after transduction in phagocytosis assays with fluorescently labeled bacteria. For selection of clonal PTPRJ-deficient HL-60 lines, single Cerulean-negative cells were sorted on a FACS AriaIII (BD Biosciences) into 96-well plates, and single-cell derived clones were expanded and analyzed for complete lack of PTPRJ by flow cytometry and Western blotting.

CEACAM3 enrichment from HL60 cell lysates

Opa_{52}-expressing *N. gonorrhoeae* were fixed in 4% paraformaldehyde-containing PBS for 20 min and then washed three times with PBS. Fixed bacteria were added to HL60 cell lysates and rotated at 4 °C for 3 h. Bacteria-bound CEACAMs were precipitated at 5000 rpm for 5 min and washed twice with PBS.

Analysis of bacterial uptake by flow cytometry

$1x10^6$ CEACAM3-mKate2-expressing HL60 cells were suspended in 1 ml phagocytosis buffer (PBS, 0.9 mM $CaCl_2$, 0.5 mM $MgCl_2$, 5 mM glucose, 1% heat-inactivated FCS). Opa_{52}-expressing *N. gonorrhoeae* (Ngo Opa_{52}) or nonopaque gonococci (Ngo Opa-) were re-suspended in 1 ml PBS, stained by addition of 2 μg/ml carboxyfluorescein succinimidyl ester (CFSE; Molecular Probes) for 20 min with constant shaking in the dark, and then washed three times with PBS (4 min, 4000 rpm). Cells were infected for the indicated time at the indicated multiplicity of infection (MOI) under gentle rotation at 37 °C. To stop bacterial uptake, samples were washed with ice-cold PBS, taken up in ice-cold phagocytosis buffer and mixed with trypan blue (final concentration 0.2 mg/ml) to quench the CFSE signal derived from extracellular bacteria (31). Bacterial uptake was analyzed by flow cytometry using a FACS Fortessa (BD Biosciences), and raw data were analyzed using FlowJo software.

CEACAM3 phosphorylation and immunoprecipitation

CEACAM3 phosphorylation was achieved either by co-transfection of 293T cells with constructs encoding the viral kinase v-Src or by infection of CEACAM3-transfected cells with Opa_{52}-expressing *N. gonorrhoeae*. Thus, depending on the assay, 293T cells were transfected to express the GFP-tagged CEACAM3 alone, or they were additionally cotransfected with v-Src-encoding constructs. If cells were not cotransfected with vSrc, they were infected with Opa_{52}-expressing *N. gonorrhoeae* (Opa_{52}) or *N. gonorrhoeae* not expressing Opa adhesins (Opa-) for 15 min 2 days after transfection (MOI 30). Transfected cells were lysed in NP40 lysis buffer containing protease and phosphatase inhibitors (10 mM p-nitrophenyl phosphate, 1 mM Na_3VO_4). CEACAM3-GFP was purified by incubation at 4 °C for 3 h with GFP-trap nanobodies (Chromotek) coupled to Sepharose beads followed by centrifugation (2700*g*, 5 min, 4 °C). The beads were washed three times with NP40 lysis buffer and taken up in 2xSDS.

Gentamicin protection assay

The day after transfection, 293T cells were seeded in triplicate into poly-L-lysine-coated 24-well plates at 5×10^5 cells/well. Next day, cells were infected for 45 min at a MOI of 30 with Opa_{52}-expressing *N. gonorrhoeae* (Opa_{52}) or *N. gonorrhoeae* that do not express Opa proteins (Opa-). Extracellular bacteria were killed by 30-min incubation in culture medium containing 100 μg/ml gentamicin. Infected cells were lysed with 0.5% (w/v) saponin in PBS for 15 min, and released bacteria were plated on GC agar plates at various dilutions. Re-isolated colony forming units (cfu) were determined, and statistical analysis of three independent experiments was performed using Student's two-tailed *t* test.

Fluorescence-based phosphatase assay with 4-MUP

Forty microliter of the recombinant purified phosphatase domains of PTPRJ or PTPRJ-D/A in phosphatase buffer (50 mM Tris HCl, pH 8.0, 150 mM NaCl, 0.01% Tween, 2 mM TCEP, and 4% BSA) were added to flat-bottomed black 384-well plates in quadruplicate. The reaction was started by adding 40 μl of 1 mM 4-MUP in phosphatase buffer (giving a final concentration of 500 μM 4-MUP). Fluorescence intensities of the hydrolyzed 4-MU (excitation 360 nm/emission 448 nm) were measured every 2 min for 60 min at 30 °C using a microplate reader (Varioscan, Thermo Fisher Scientific).

In vitro *phosphatase assay with malachite green*

In vitro phosphatase assays were performed with CEACAM3 phospho-peptides synthesized by Novopep: CEACAM3-pY230: (Biotin-LPNPRTAASI[pY]EELLKHDTNIY CRMDHKAEVAS) or CEACAM3-pY241: (Biotin-LPNPRTA ASIYEELLKHDTNI[pY]CRMDHKAEVAS). Recombinant 6xHis-Sumo-labeled phosphatase domains of PTPRJ or PTPRJ-D/A were incubated at 30 °C under constant shaking with 100 μM CEACAM3 phospho-peptides in phosphatase buffer (50 mM Tris HCl, pH 8.0, 150 mM NaCl, 0.01% Tween20, 2 mM TCEP). After 60 min (or after the indicated time), the reaction was stopped by adding the same volume of malachite green solution (54 mM NH_4Mo, 0.9 mM malachite green in 1 M HCl). $A_{615\ nm}$ was measured using a microplate reader (Varioscan, Thermo Fisher Scientific).

Immunofluorescence staining and confocal microscopy

For colocalization experiments, 2 x 10^5 293T cells were cotransfected with expression plasmids encoding for GFP-tagged wildtype CEACAM3 or GFP alone together with mScarlet, mScarlet-tagged myristoylated PTPRJ, or PTPRJ-D/A. Cells were seeded onto poly-L-lysine-coated coverslips and allowed to adhere for 2 h. Opa_{52}-expressing *N. gonorrhoeae* were suspended in PBS and stained with 4 μg/ml PacificBlue-NHS (Molecular Probes). After washing the bacteria three

times with PBS, the adherent cells were infected with MOI 30 for 1 h. The infected samples were washed with PBS and fixed with 4% PFA in PBS for 20 min. Coverslips were washed three times with PBS and mounted on glass slides using Dako Mounting Medium (Dako). Finally, samples were imaged using a Leica SP5 confocal microscope, and images were digitally processed using ImageJ.

To compare the surface expression of PTPRJ in HL60-CEACAM3-mKate control cells (sgCer) with that in the HL60-CEACAM3-mKate-sgPTPRJ cells (sgPTPRJ), 5 x 10^5 cells each were seeded in 1 ml PBS in 24-well plates with poly-L-lysine-coated coverslips and allowed to sink to the bottom of the wells by centrifugation at 800 rpm for 4 min. The PBS was aspirated, and samples were fixed with 4% PFA-containing PBS for 20 min, washed three times with PBS, and blocked with blocking solution (10% heat-inactivated FCS in PBS) for 5 min. Cells were stained for 1 h with an α-PTPRJ antibody (clone 143–41, Santa Cruz; 1:100) or an IgG isotype control antibody in blocking solution. After washing with PBS and blocking with blocking solution for 5 min, cells were treated with an Alexa Fluor 488-conjugated secondary goat anti-mouse antibody (1:200) for 45 min in the dark. In addition, Hoechst33342 was added 15 min before the end of the 45-min incubation period to stain nuclear DNA. Samples were washed three times with PBS and mounted on coverslips as previously described.

Immunofluorescence staining for FACS analysis

1 x 10^6 cells were taken up in FACS buffer (5% FCS in PBS) and transferred to Eppendorf tubes. Cells were centrifuged at 2.500 rpm for 2 min at 4 °C and incubated with the desired concentration of the primary antibody in FACS buffer for 1 h on ice. Samples were washed three times with FACS buffer and were then incubated with the fluorescently labeled secondary antibody in FACS buffer for 30 min at 4 °C in the dark. Cells were washed as before, suspended in 600 µl FACS buffer, and transferred to FACS tubes. Finally, cells were analyzed by flow cytometry (BD LSRII, FACSDiva software; BD Biosciences), and obtained data were evaluated using the FlowJo software package.

Scanning electron microscopy

HL60 cells were seeded at 4 x 10^4 cells/well in phagocytosis buffer on 12 mm glass coverslips coated with poly-L-lysine (10 mg/ml). Cells were infected for 30 min with Opa_{52}-expressing *N. gonorrhoeae* at an MOI of 30 or were left uninfected. Samples were fixed at 4 °C for a total of 60 min in EM-fixative (0.1 M Hepes, pH 7.2, 3% formaldehyde, 2% glutaraldehyde, 0.09 M sucrose, 0.01 M $CaCl_2$, 0.01 M $MgCl_2$) that was renewed one time. Fixed samples were washed three times with washing buffer (0.1 M Hepes, pH 7.2, 0.09 M sucrose, 0.01 M $CaCl_2$, 0.01 M $MgCl_2$) and dehydrated in an ethanol gradient, critical point dried with liquid CO_2 (BAL-TEC SCD 030 Critical Point Dryer), and sputter-coated with 8 mm gold-palladium. Samples were imaged at 5 kV in a field emission scanning electron microscope (Auriga; Carl Zeiss AG). To estimate the size of lamellipodia, raw SEM images were opened in NIH ImageJ and the circumference of lamellipodia from individual cells was marked with the "region of interest selection" tool. For each lamellipodium, the area in μm^2 was determined.

Statistics

Data are presented as mean ± SEM or mean ± SD as indicated in the figure legend. Statistical significance was determined with either a two-tailed Student's *t* test or a one-way ANOVA followed by a Dunnett's posttest, using Prism5 (GraphPad). The significance level was set at $p < 0.05$ and is indicated by $^*p < 0.05$; $^{**}p < 0.01$; $^{***}p < 0.001$; or ns, not significant. Further statistical details are provided in the figures and figure legends.

Data availability

All data relevant to this study are included within this manuscript.

Supporting information—This article contains supporting information.

Acknowledgments—We thank I. Royal (University of Montreal, Canada) for providing full-length cDNA of PTPRJ, our VTK students Franziska Grathwol and Katja Kümmerlen (University of Konstanz) and S. Feindler-Boeckh for expert technical assistance. We are grateful to the Flow Cytometry center Konstanz (FlowKon) and Michael Laumann (Electron Microscopy Service of the Department of Biology, University of Konstanz) for technical support.

Author contributions—G. G., J. A., and C. R. H. conceptualization; G. G., J. A., and C. C. investigation; G. G., J. A. methodology; G. G. and C. R. H. writing; C. R. H. funding acquisition; C. R. H. supervision.

Funding and additional information—This study was supported by funds from the Deutsche Forschungsgemeinschaft (Ha 2856/10–1) to C. R. H. The funding body was not involved in the design, in the collection, analysis, and interpretation of data; in the writing of the manuscript; nor in the decision to submit the manuscript for publication.

Conflict of interest—The authors declare that they have no conflicts of interest with the contents of this article.

Abbreviations—The abbreviations used are: CEACAM, carcinoembryonic antigen-related cell adhesion molecule; CFSE, carboxyfluorescein succinimidyl ester; FCS, fetal calf serum; ITAM, immunoreceptor tyrosine-based activation motif; Ig, immunoglobulin; LIC, ligation independent cloning; MOI, multiplicity of infection; 4-MUP, 4-methylumbelliferyl phosphate; PTPR, receptor-type protein tyrosine phosphatase; PTK, protein tyrosine kinase; sgRNA, single guide RNA.

References

1. Janeway, C. A., Jr., and Medzhitov, R. (2002) Innate immune recognition. *Annu. Rev. Immunol.* **20**, 197–216

2. Underhill, D. M., and Ozinsky, A. (2002) Phagocytosis of microbes: complexity in action. *Annu. Rev. Immunol.* **20**, 825–852
3. Goodridge, H. S., Underhill, D. M., and Touret, N. (2012) Mechanisms of Fc receptor and dectin-1 activation for phagocytosis. *Traffic* **13**, 1062–1071
4. Bonsignore, P., Kuiper, J. W. P., Adrian, J., Goob, G., and Hauck, C. R. (2020) CEACAM3-A Prim(at)e invention for opsonin-independent phagocytosis of bacteria. *Front. Immunol.* **10**, 3160
5. Adrian, J., Bonsignore, P., Hammer, S., Frickey, T., and Hauck, C. R. (2019) Adaptation to host-specific bacterial pathogens drives rapid evolution of a human innate immune receptor. *Curr. Biol.* **29**, 616–630.e5
6. Pils, S., Gerrard, D., Meyer, A., and Hauck, C. R. (2008) CEACAM3: an innate immune receptor directed against human-resticted bacterial pathogens. *Int. J. Med. Microbiol.* **298**, 553–560
7. Schmitter, T., Agerer, F., Peterson, L., Muenzner, P., and Hauck, C. R. (2004) Granulocyte CEACAM3 is a phagocytic receptor of the innate immune system that mediates recognition and elimination of human-specific pathogens. *J. Exp. Med.* **199**, 35–46
8. Roth, A., Mattheis, C., Münzner, P., Unemo, M., and Hauck, C. R. (2013) Innate recognition by neutrophil granulocytes differs between *Neisseria gonorrhoeae* strains causing local or disseminating infections. *Infect. Immun.* **81**, 2358–2370
9. Hill, D. J., and Virji, M. (2003) A novel cell-binding mechanism of *Moraxella catarrhalis* ubiquitous surface protein UspA: specific targeting of the N-domain of carcinoembryonic antigen-related cell adhesion molecules by UspA1. *Mol. Microbiol.* **48**, 117–129
10. Tchoupa, A. K., Lichtenegger, S., Reidl, J., and Hauck, C. R. (2015) Outer membrane protein P1 is the CEACAM-binding adhesin of *Haemophilus influenzae*. *Mol. Microbiol.* **98**, 440–455
11. Koniger, V., Holsten, L., Harrison, U., Busch, B., Loell, E., Zhao, Q., *et al.* (2016) Helicobacter pylori exploits human CEACAMs *via* HopQ for adherence and translocation of CagA. *Nat. Microbiol.* **2**, 16188
12. McCaw, S. E., Schneider, J., Liao, E. H., Zimmermann, W., and Gray-Owen, S. D. (2003) Immunoreceptor tyrosine-based activation motif phosphorylation during engulfment of *Neisseria gonorrhoeae* by the neutrophil-restricted CEACAM3 (CD66d) receptor. *Mol. Microbiol.* **49**, 623–637
13. Schmitter, T., Pils, S., Sakk, V., Frank, R., Fischer, K. D., and Hauck, C. R. (2007) The granulocyte receptor CEACAM3 directly associates with Vav to promote phagocytosis of human pathogens. *J. Immunol.* **178**, 3797–3805
14. Pils, S., Kopp, K., Peterson, L., Delgado-Tascon, J., Nyffenegger-Jann, N. J., and Hauck, C. R. (2012) The adaptor molecule Nck localizes the WAVE complex to promote actin polymerization during CEACAM3-mediated phagocytosis of bacteria. *PLoS One* **7**, e32808
15. Sarantis, H., and Gray-Owen, S. D. (2012) Defining the roles of human carcinoembryonic antigen-related cellular adhesion molecules during neutrophil responses to Neisseria gonorrhoeae. *Infect. Immun.* **80**, 345–358
16. Billker, O., Popp, A., Brinkmann, V., Wenig, G., Schneider, J., Caron, E., *et al.* (2002) Distinct mechanisms of internalization of *Neisseria gonorrhoeae* by members of the CEACAM receptor family involving Rac1- and Cdc42- dependent and -independent pathways. *EMBO J.* **21**, 560–571
17. Buntru, A., Roth, A., Nyffenegger-Jann, N. J., and Hauck, C. R. (2012) HemITAM signaling by CEACAM3, a human granulocyte receptor recognizing bacterial pathogens. *Arch. Biochem. Biophys.* **524**, 77–83
18. Sarantis, H., and Gray-Owen, S. D. (2007) The specific innate immune receptor CEACAM3 triggers neutrophil bactericidal activities *via* a Syk kinase-dependent pathway. *Cell Microbiol.* **9**, 2167–2180
19. Buntru, A., Kopp, K., Voges, M., Frank, R., Bachmann, V., and Hauck, C. R. (2011) Phosphatidylinositol-3' kinase activity is critical for initiating the oxidative burst and bacterial destruction during CEACAM3-mediated phagocytosis. *J. Biol. Chem.* **286**, 9555–9566
20. Furukawa, T., Itoh, M., Krueger, N. X., Streuli, M., and Saito, H. (1994) Specific interaction of the CD45 protein-tyrosine phosphatase with tyrosine-phosphorylated CD3 zeta chain. *Proc. Natl. Acad. Sci. U. S. A.* **91**, 10928–10932
21. Baker, J. E., Majeti, R., Tangye, S. G., and Weiss, A. (2001) Protein tyrosine phosphatase CD148-mediated inhibition of T-cell receptor signal transduction is associated with reduced LAT and phospholipase Cgamma1 phosphorylation. *Mol. Cell Biol.* **21**, 2393–2403
22. Cordoba, S. P., Choudhuri, K., Zhang, H., Bridge, M., Basat, A. B., Dustin, M. L., *et al.* (2013) The large ectodomains of CD45 and CD148 regulate their segregation from and inhibition of ligated T-cell receptor. *Blood* **121**, 4295–4302
23. Boggon, T. J., and Eck, M. J. (2004) Structure and regulation of Src family kinases. *Oncogene* **23**, 7918–7927
24. Hermiston, M. L., Zikherman, J., and Zhu, J. W. (2009) CD45, CD148, and Lyp/Pep: critical phosphatases regulating Src family kinase signaling networks in immune cells. *Immunol. Rev.* **228**, 288–311
25. Stepanek, O., Kalina, T., Draber, P., Skopcova, T., Svojgr, K., Angelisova, P., *et al.* (2011) Regulation of Src family kinases involved in T cell receptor signaling by protein-tyrosine phosphatase CD148. *J. Biol. Chem.* **286**, 22101–22112
26. Goodridge, H. S., Reyes, C. N., Becker, C. A., Katsumoto, T. R., Ma, J., Wolf, A. J., *et al.* (2011) Activation of the innate immune receptor Dectin-1 upon formation of a 'phagocytic synapse'. *Nature* **472**, 471–475
27. Takahashi, T., Takahashi, K., St John, P. L., Fleming, P. A., Tomemori, T., Watanabe, T., *et al.* (2003) A mutant receptor tyrosine phosphatase, CD148, causes defects in vascular development. *Mol. Cell Biol.* **23**, 1817–1831
28. Marconi, C., Di Buduo, C. A., LeVine, K., Barozzi, S., Faleschini, M., Bozzi, V., *et al.* (2019) Loss-of-function mutations in PTPRJ cause a new form of inherited thrombocytopenia. *Blood* **133**, 1346–1357
29. Senis, Y. A., Tomlinson, M. G., Ellison, S., Mazharian, A., Lim, J., Zhao, Y., *et al.* (2009) The tyrosine phosphatase CD148 is an essential positive regulator of platelet activation and thrombosis. *Blood* **113**, 4942–4954
30. Mori, J., Wang, Y. J., Ellison, S., Heising, S., Neel, B. G., Tremblay, M. L., *et al.* (2012) Dominant role of the protein-tyrosine phosphatase CD148 in regulating platelet activation relative to protein-tyrosine phosphatase-1B. *Arterioscler Thromb. Vasc. Biol.* **32**, 2956–2965
31. Pils, S., Schmitter, T., Neske, F., and Hauck, C. R. (2006) Quantification of bacterial invasion into adherent cells by flow cytometry. *J. Microbiol. Methods* **65**, 301–310
32. Rincon, E., Rocha-Gregg, B. L., and Collins, S. R. (2018) A map of gene expression in neutrophil-like cell lines. *BMC Genomics* **19**, 573
33. Schmitter, T., Pils, S., Weibel, S., Agerer, F., Buntru, A., Kopp, K., *et al.* (2007) Opa proteins of pathogenic *Neisseriae* initiate Src-kinase-dependent or lipid raft-mediated uptake via distinct human CEACAM isoforms. *Infect. Immun.* **75**, 4116–4126
34. Kopp, K., Buntru, A., Pils, S., Zimmermann, T., Frank, R., Zumbusch, A., *et al.* (2012) GRB14 is a negative regulator of ceacam3-mediated phagocytosis of pathogenic bacteria. *J. Biol. Chem.* **287**, 39158–39170
35. Arora, D., Stopp, S., Bohmer, S. A., Schons, J., Godfrey, R., Masson, K., *et al.* (2011) Protein-tyrosine phosphatase DEP-1 controls receptor tyrosine kinase FLT3 signaling. *J. Biol. Chem.* **286**, 10918–10929
36. Hermiston, M. L., Xu, Z., and Weiss, A. (2003) CD45: a critical regulator of signaling thresholds in immune cells. *Annu. Rev. Immunol.* **21**, 107–137
37. Godfrey, R., Arora, D., Bauer, R., Stopp, S., Muller, J. P., Heinrich, T., *et al.* (2012) Cell transformation by FLT3 ITD in acute myeloid leukemia involves oxidative inactivation of the tumor suppressor protein-tyrosine phosphatase DEP-1/PTPRJ. *Blood* **119**, 4499–4511
38. den Hertog, J., Ostman, A., and Bohmer, F. D. (2008) Protein tyrosine phosphatases: regulatory mechanisms. *FEBS J.* **275**, 831–847
39. Sintsova, A., Sarantis, H., Islam, E. A., Sun, C. X., Amin, M., Chan, C. H., *et al.* (2014) Global analysis of neutrophil responses to Neisseria gonorrhoeae reveals a self-propagating inflammatory program. *PLoS Pathog.* **10**, e1004341
40. Heinrich, A., Heyl, K. A., Klaile, E., Muller, M. M., Klassert, T. E., Wiessner, A., *et al.* (2016) *Moraxella catarrhalis* induces CEACAM3-

Syk-CARD9-dependent activation of human granulocytes. *Cell Microbiol.* **18**, 1570–1582
41. Achtman, M., Neibert, M., Crowe, B. A., Strittmatter, W., Kusecek, B., Weyse, E., *et al.* (1988) Purification and characterization of eight class 5 outer membrane protein variants from a clone of Neisseria meningitidis serogroup A. *J. Exp. Med.* **168**, 507–525
42. Grimm, T. M., Dierdorf, N. I., Betz, K., Paone, C., and Hauck, C. R. (2020) PPM1F controls integrin activity *via* a conserved phospho-switch. *J. Cell Biol.* **219**, e202001057
43. Kupsch, E.-M., Knepper, B., Kuroki, T., Heuer, I., and Meyer, T. F. (1993) Variable opacity (Opa) outer membrane proteins account for the cell tropisms displayed by *Neisseria gonorrhoeae* for human leukocytes and epithelial cells. *EMBO J.* **12**, 641–650
44. Sanjana, N. E., Shalem, O., and Zhang, F. (2014) Improved vectors and genome-wide libraries for CRISPR screening. *Nat. Methods* **11**, 783–784
45. Spring, K., Chabot, C., Langlois, S., Lapointe, L., Trinh, N. T., Caron, C., *et al.* (2012) Tyrosine phosphorylation of DEP-1/CD148 as a mechanism controlling Src kinase activation, endothelial cell permeability, invasion, and capillary formation. *Blood* **120**, 2745–2756
46. Andreasson, C., Fiaux, J., Rampelt, H., Mayer, M. P., and Bukau, B. (2008) Hsp110 is a nucleotide-activated exchange factor for Hsp70. *J. Biol. Chem.* **283**, 8877–8884